

## NEUROSCIENCE

# Social transmission of food safety depends on synaptic plasticity in the prefrontal cortex

Michaël Loureiro<sup>1</sup>, Ridouane Achargui<sup>1</sup>, Jérôme Flakowski<sup>1</sup>, Ruud Van Zessen<sup>1</sup>, Thomas Stefanelli<sup>1</sup>, Vincent Pascoli<sup>1</sup>, Christian Lüscher<sup>1,2\*</sup>

When an animal is facing unfamiliar food, its odor, together with semiochemicals emanating from a conspecific, can constitute a safety message and authorize intake. The piriform cortex (PiC) codes olfactory information, and the inactivation of neurons in the nucleus accumbens (NAc) can acutely trigger consumption. However, the neural circuit and cellular substrate of transition of olfactory perception into value-based actions remain elusive. We detected enhanced activity after social transmission between two mice in neurons of the medial prefrontal cortex (mPFC) that target the NAc and receive projections from the PiC. Exposure to a conspecific potentiated the excitatory postsynaptic currents in NAc projectors, whereas blocking transmission from PiC to mPFC prevented social transmission. Thus, synaptic plasticity in the mPFC is a cellular substrate of social transmission of food safety.

**A**lthough metabolic needs ultimately drive food consumption, additional factors determine the moment-to-moment intake. For example, a predator threat may halt eating even when hungry. Conversely, when palatable foods are found, prolonged consumption can occur, leading to accumulation of fat storage (1). Moreover, many species use information acquired from peers to decide whether food is safe to eat. Whereas primates rely predominantly on visual cues, rodents use their olfactory system to detect odors, including carbon disulfide (CS<sub>2</sub>), a semiochemical component of the rodent breath (2, 3). Such social transmission of food preference (STFP) occurs when an observer mouse exposed to a demonstrator mouse fed with scented food drives a preference for that food over a differently scented alternative (4). Recent studies demonstrate the involvement of olfactory sensory neurons and mitral cells in the olfactory bulb for STFP acquisition (5), which project to the piriform cortex (PiC). The activity of neurons in the medial prefrontal cortex (mPFC) increases substantially in response to reward-predicting cues (6), which may drive decision-making processes (7) by cells that project to the nucleus accumbens (NAc projectors). From there, D1R-expressing neurons, a major inhibitory output of the NAc, could control the food intake on a rapid time scale independently of metabolic needs (8).

Rodents exposed simultaneously to cumin- and thyme-flavored food exhibit an innate preference for the thyme option (9). We first confirmed that observer mice cued by a demonstrator fed with

cumin-flavored food increased their time exploring and eating the cumin-scented option, without affecting the total amount of food eaten (fig. s1, A to F). STFP acquisition was efficient only if the food options were unfamiliar to cued observers (fig. s1, G to I), corroborating the transmission of a safety signal, rather than passing a mere preference. We then monitored the activity of neurons projecting to the NAc projectors in the mPFC and the paraventricular nucleus of the thalamus (PVT), involved in decision making (10) and the expression of aversive memories (11), respectively. To identify NAc projectors, we injected cholera toxin subunit B (CTB) into the NAc of observer mice and quantified cFos expression, a proxy for neuronal activity, after conspecific interaction or the food choice session (Fig. 1, A to C). These manipulations did not affect the interaction between demonstrator and observer mice nor the concomitant cFos expression in NAc projectors (Fig. 1D). However, when quantified immediately after food choice sessions, cFos-positive mPFC NAc projectors (but not the overall number of cFos-positive neurons in the mPFC; fig. s2, C and D) were more abundant in cued mice compared with uncued mice, an effect not observed in PVT NAc projectors (Fig. 1E) despite a similar density of NAc projectors to the two structures (fig. s2, A and B). The amount of food consumed by uncued and cued animals was similar and therefore could not explain the change in mPFC NAc projectors engagement between groups (fig. s2E). We next determined the functional consequences onto medium-sized spiny neurons (MSNs) in the NAc. To record transmission selectively from these synapses, we injected *Fos*<sup>creER/T2</sup>-transgenic mice in the mPFC with a cre-inducible adeno-associated virus (AAV) containing channelrhodopsin (ChR2), along with mCherry for visualization (AAV-DIO-ChR2-mCherry) (Fig. 1, F to H, and fig. s2, F and G).

*Fos*<sup>creER/T2</sup> mice provide a *fos*-dependent labeling of active population when 4-hydroxytamoxifen (4-OHT) is present in the brain (12, 13). Although the density of mPFC cells expressing ChR2-mCherry was similar in cued and uncued mice (Fig. 1H), we observed excitatory postsynaptic currents (EPSCs) in 36% of MSNs (39.4 pA on average) in mice exposed to a demonstrator but in only 19% of MSNs (20.9 pA on average) in uncued controls (Fig. 1I). This difference in connectivity and amplitude was not observed in mice injected with a cre-independent AAV-ChR2-EYFP (enhanced yellow fluorescent protein) virus in the mPFC (fig. s2, H to J). We next tested whether chemogenetic inhibition of mPFC NAc projectors during the food choice session could affect STFP expression. We injected the NAc of observer mice with a retrograde AAV that virally expresses the Cre recombinase (AAV2rg-pkg-Cre), followed by an injection in the mPFC of an AAV that expresses the hM4D(Gi) receptor in a cre-dependent manner (Fig. 1J). Injection of clozapine-n-oxide (CNO) in the absence of hM4D(Gi) receptors did not affect the preference of the observers. However, the inhibition of mPFC NAc projectors in cued animals abolished STFP expression (Fig. 1, K and L).

Because STFP induction requires CS<sub>2</sub>, a component of the mouse breath (2), we mimicked the switch in food preference by simultaneously exposing mice to CS<sub>2</sub> and cumin-flavored food (fig. s3, A to C). Odors are encoded in the PiC and a single brief exposure to CS<sub>2</sub> increases the number of cFos-positive neurons (fig. s3, D to F), suggesting the involvement of the PiC in STFP acquisition. Given the above results implicating mPFC NAc projectors for STFP expression, we searched for a direct connection between the two brain regions. To test whether mPFC NAc projectors receive monosynaptic inputs from the PiC, we used the retrograde transsynaptic and rabies-based method TRIO (“tracing the relationship between input and output”) (14). C57BL6/J mice were injected with retrograde AAV2rg-pkg-Cre in the NAc and helper AAVs in the mPFC, allowing the Cre-dependent expression of the TVA receptor for EnvA fused with mCherry and the rabies glycoprotein (G) (Fig. 2A). One month later, glycoprotein-deleted and green fluorescent protein-expressing rabies viruses (RVdG) were injected in the mPFC and efficiently infected NAc projectors (Fig. 2B). Analysis of distal inputs to mPFC NAc projectors revealed major connections from the posterior part of the PiC, as well as from other regions such as the mediodorsal thalamus and the basolateral amygdala (Fig. 2, C and D). We confirmed the synaptic connectivity between PiC neurons and mPFC NAc projectors in acute brain slices. We injected an AAV-ChR2-EYFP in the PiC and optogenetically stimulated its terminals in the mPFC while recording from NAc projectors (CTB-555-positive cells; Fig. 2, E and F). When clamped at -70 mV, we found EPSCs in 76% of NAc projectors, with an average amplitude of 274 ± 23 pA and a membrane capacitance of 116 ± 5 pF, suggesting that most of the recorded cells were

<sup>1</sup>Department of Basic Neurosciences, Medical Faculty, University of Geneva, CH-1211 Geneva, Switzerland. <sup>2</sup>Clinic of Neurology, Department of Clinical Neurosciences, Geneva University Hospital, CH-1211 Geneva, Switzerland.

\*Corresponding author. Email: christian.luscher@unige.ch

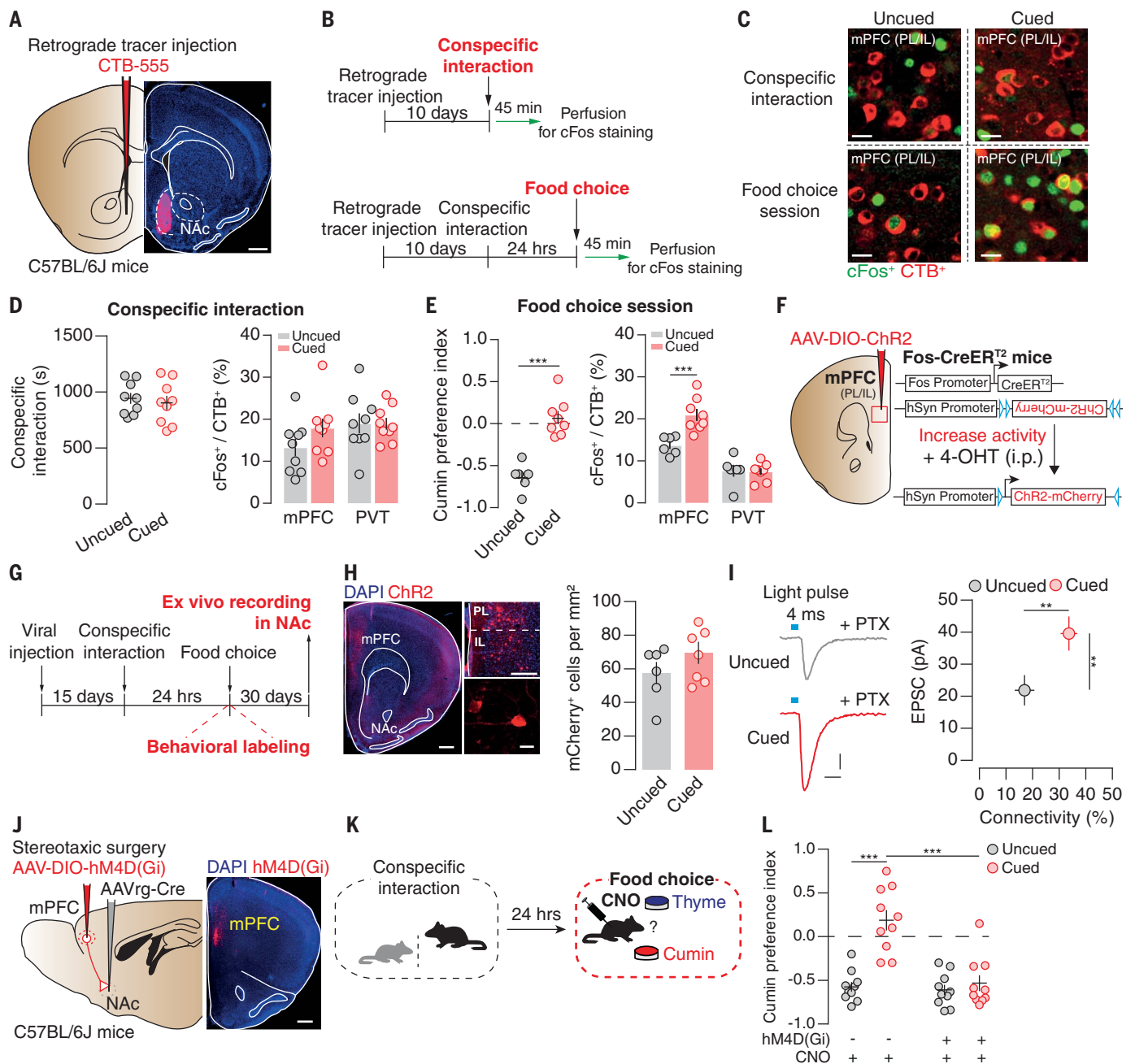


**Fig. 1. Implication of mPFC NAc projectors in STFP expression.**

(A) Expression of the retrograde tracer CTB-555 in the NAc. Scale bar, 500  $\mu\text{m}$ . (B) Mice were perfused either after conspecific interactions (top) or after the food choice session (bottom). (C) Histological example of mPFC NAc projectors (red, CTB-positive) and cFos expression. Yellow cells are mPFC NAc projectors activated during behavior. Scale bars: 20  $\mu\text{m}$ . (D) Left: time spent by uncued and cued mice with the demonstrators during the conspecific interaction session before perfusion. Right: cFos quantification in NAc projectors in the mPFC and PVT. (E) Left: cumin preference index = (time in cumin food zone – time in thyme food zone)/(time in cumin food zone + time in thyme food zone). Mice cued by a demonstrator fed with cumin showed an increase preference for cumin-flavored food compared with uncued mice ( $***p < 0.001$ ). Right: cFos quantification in the mPFC and PVT NAc projectors after the food choice session. The density of mPFC NAc projectors activated was significantly higher in cued mice compared with uncued animals ( $***p < 0.01$ ). No difference was observed for PVT NAc projectors. (F) *Fos-Cre<sup>ER/T2</sup>* mice were injected with AAV<sub>DJ</sub>-hSyn-DIO-ChR2-mCherry

in the mPFC to express ChR2 under the control of the *fos* promoter and the presence of 4-OHT (10 mg/kg). (G) Experimental timeline. Mice were injected 4-OHT immediately after the food choice session. (H) Left: example of ChR2-mCherry-infected neurons in the mPFC. Scale bars: left, 500  $\mu\text{m}$ ; top right, 250  $\mu\text{m}$ ; bottom right, 20  $\mu\text{m}$ . Right: The density of mPFC neurons expressing ChR2 was similar between uncued and cued animals. (I) Left: example of light-evoked current recorded in uncued (gray) or cued (red) observers. Scale bars: 20 pA, 10 ms. Right: connectivity plot summarizing NAc neurons receiving excitatory inputs from mPFC neurons activated during the food choice session (uncued:  $n = 63$  cells from six mice; cued:  $n = 80$  cells from seven mice;  $**p < 0.01$ ). (J) Viral strategy with histological examples for chemogenetic inhibition of mPFC-to-NAc pathway. Scale bar, 500  $\mu\text{m}$ . (K) CNO injections (2 mg/kg, ip) were performed 60 min before the food choice session in uncued and cued observers. (L) Impact of mPFC-to-NAc pathway inhibition during the food choice session on the cumin preference score. See tables S1 and S2 for complete statistics and mean  $\pm$  SEM values, respectively.

pyramidal neurons (Fig. 2, G to J). The sodium channel blocker tetrodotoxin (TTX) reduced but did not abolish EPSC amplitudes, indicating a monosynaptic connection. The AMPA/kainate receptor antagonist 2,3-dihydroxy-6-nitro-7-sulfamoylbenzo[*f*]quinoxaline (NBQX) blocked the residual EPSCs (Fig. 2K). When NAc projectors were voltage clamped at 0 mV, light stimulation evoked prominent inhibitory postsynaptic currents (IPSCs; average amplitude  $732 \pm 47$  pA), albeit with a longer onset delay than that of EPSCs (Fig. 2, L to N). IPSCs were completely blocked by the  $\gamma$ -aminobutyric acid type A (GABA<sub>A</sub>) receptor antagonist picrotoxin

(PTX) or by TTX (Fig. 2O). In addition, bath application of NBQX also abolished light-evoked IPSCs.

We next investigated whether STFP acquisition would modify the properties of PiC-to-mPFC NAc-projector synapses. Observer mice expressing Chr2-EYFP in PiC neurons and CTB-555 in mPFC NAc projectors were exposed to demonstrator mice fed with cumin-flavored or regular chow. Because feeding could affect synaptic transmission, mPFC slices from observers were prepared for ex vivo recordings of synaptic currents in NAc projectors without being tested for the observers' food preference (Fig. 3A). Although both groups of mice explored the demonstrators for a similar

duration (Fig. 3, B and C), optogenetic stimulation of PiC terminals in the mPFC revealed a higher EPSC to IPSC ratio in NAc projectors from cued mice compared with uncued or naïve animals, an effect not observed in unlabeled mPFC cells, likely to project elsewhere (Fig. 3D). The paired-pulse ratio of EPSCs and IPSCs (fig. s4, A to E) and the rectification index of AMPA receptor EPSCs (Fig. 3F), a measure of calcium permeability (15), were similar in the three groups. Comparing light-evoked AMPA-EPSCs and *N*-methyl-D-aspartate (NMDA)-EPSCs from uncued and cued mice revealed a significantly higher AMPA/NMDA ratio in cued mice (Fig. 3E).

## Fig. 2. The connection from the PiC-to-mPFC NAc projectors is monosynaptic and excitatory.

(A) Schematic of a rabies-based TRIO strategy from NAc projectors in the mPFC.

(B) Starter cells in the mPFC (PL: prelimbic; IL: infralimbic; cc: corpus callosum).

Scale bars: left, 500  $\mu$ m; right, 25  $\mu$ m.

(C) Example of distal inputs to mPFC NAc projectors (MD: mediodorsal thalamus; SMT: submedius thalamus; BLA: basolateral amygdala). Scale bar, 1 mm.

(D) Higher magnification of the MD, BLA, and PiC.

(E) Viral injection strategy to record (ex vivo whole-cell voltage-clamp recording) mPFC NAc projectors and to optogenetically stimulate PiC terminals in the mPFC. Scale bars, 500  $\mu$ m.

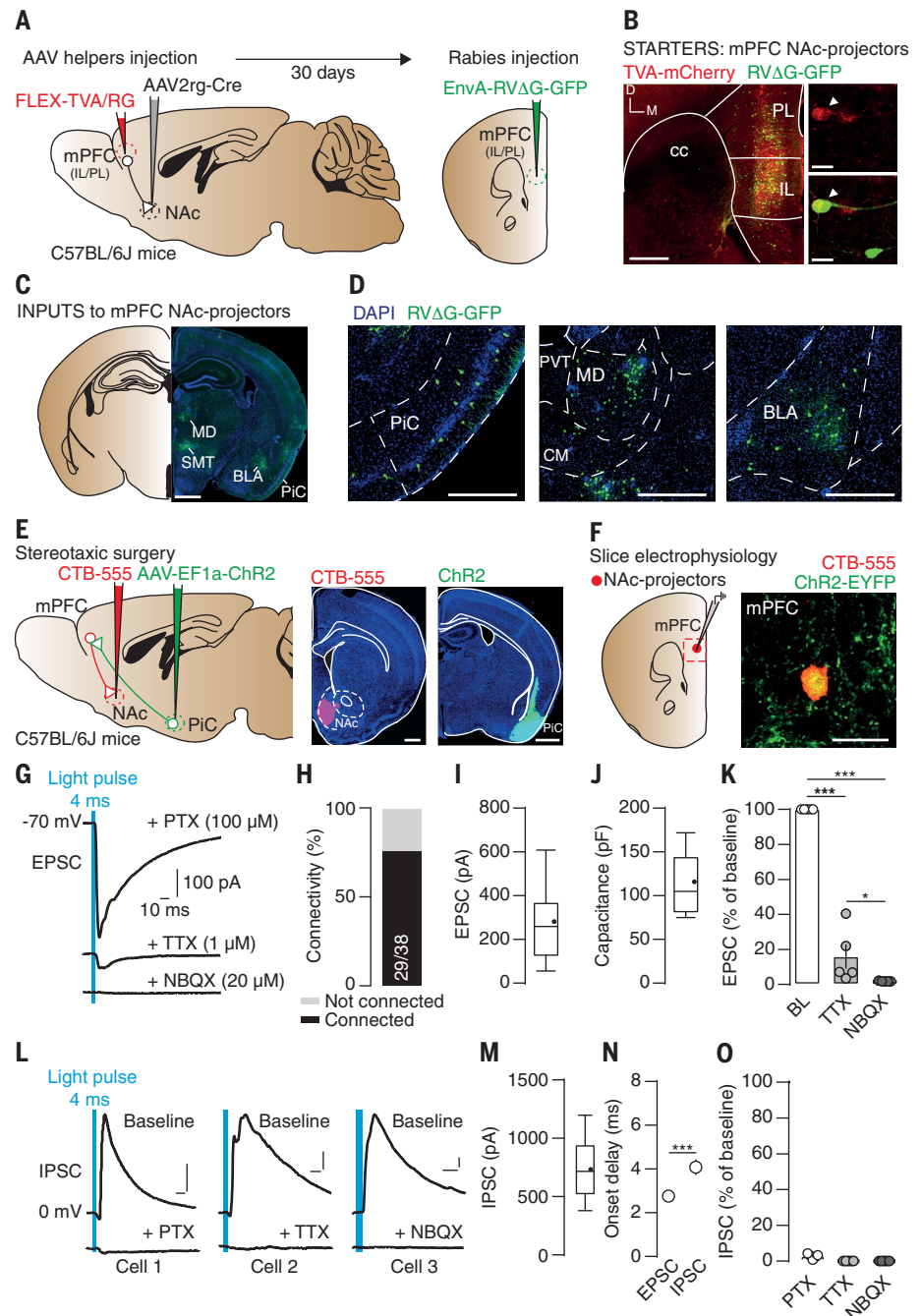
(F) Histological image showing a recorded mPFC NAc projector. Note the surrounding PiC fibers expressing Chr2. Scale bar: 20  $\mu$ m.

(G) Example traces of light-induced EPSC. Scale bars: 100 pA, 10 ms.

(H) Connectivity between PiC and mPFC NAc projectors. (I) EPSC amplitudes.

(J) Capacitance. (K) EPSC amplitudes were reduced after bath application of TTX (a voltage-gated Na<sup>+</sup> channel blocker) and completely blocked by bath application of NBQX (an AMPAR blocker).

(L) IPSC example traces. Scale bars: 100 pA, 10 ms. (M) The onset delay was longer for recorded IPSCs compared with EPSCs. (N) IPSC amplitudes. (O) IPSCs were completely blocked by PTX (a GABA<sub>A</sub> receptor antagonist) or TTX and NBQX. Box plot represents data as median with 25th to 75th percentile (box) and minimum–maximum (whiskers); black dots represent the mean of the group. Histograms represent mean  $\pm$  SEM and circles individual cells. \**p* < 0.05; \*\*\**p* < 0.001. See tables S1 and S2 for complete statistics and mean  $\pm$  SEM values, respectively.



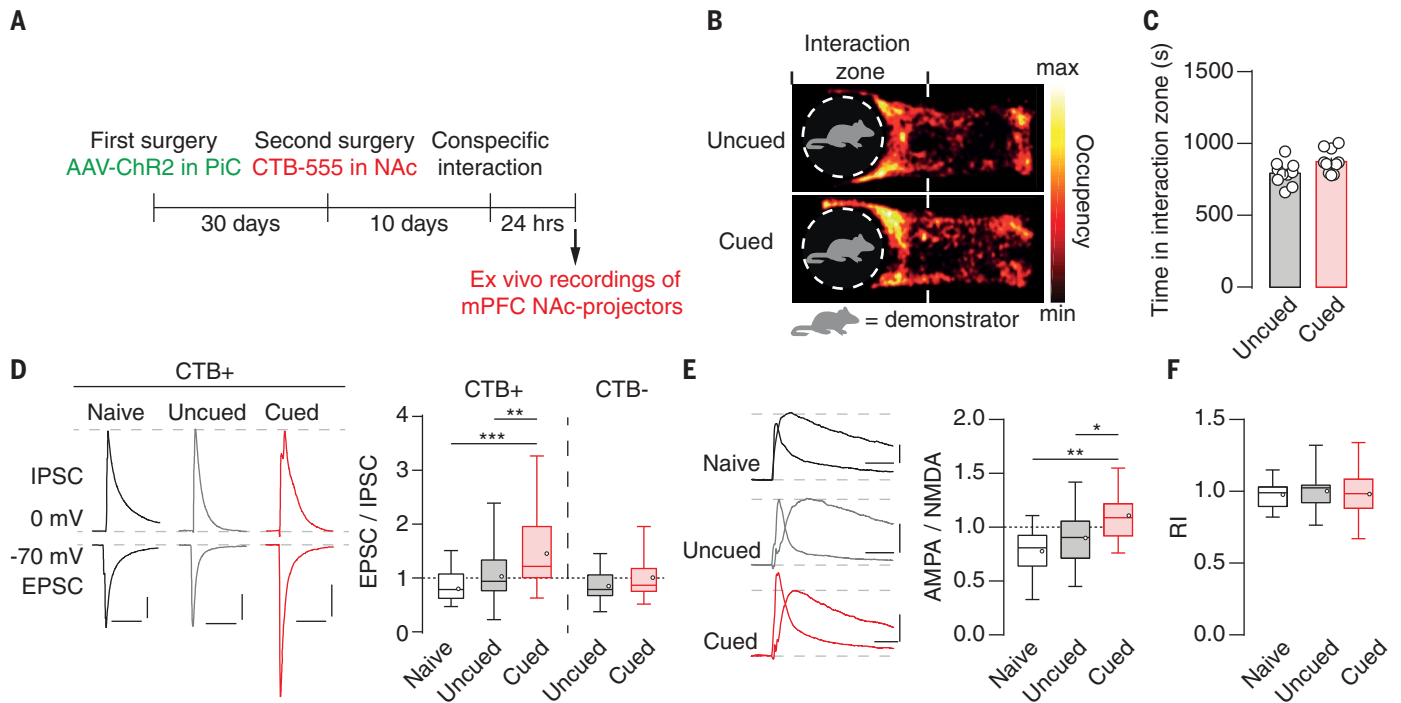


**Fig. 3. STFP acquisition increases the excitatory transmission at PiC-to-mPFC NAc projectors.** (A) Observer mice were perfused 24 hours after conspecific interaction for ex vivo recordings of light-evoked current in mPFC NAc projectors. (B) Representative occupancy heat maps of the time spent by an uncued or cued observer during conspecific interaction. (C) The time spent by uncued and cued observers in the interaction zone was not different. Black crosses represent mean  $\pm$  SEM. (D) Example traces of IPSC and EPSC amplitude in mPFC NAc projectors (left) and grouped data for EPSC/IPSC ratios (right).  $n = 31$  cells per group (five mice per

group). Scale bars: 200 pA, 100 ms. (E) Example traces of AMPAR and NMDA-EPSCs recorded at +40 mV (left) and grouped data for AMPA/NMDA ratio (right). Scale bars: 100 pA, 50 ms.  $n = 13, 17,$  and  $20$  cells recorded in the naive ( $n = 4$  mice), uncued ( $n = 5$  mice), and cued ( $n = 5$  mice) groups, respectively. (F) Grouped data for the rectification index. Box plot represents data as median with 25/75 percentile (box) and minimum–maximum (whiskers); open circles represent the mean of the group. Histograms represent mean  $\pm$  SEM.  $**p < 0.01$ ;  $***p < 0.001$ . See tables S1 and S2 for complete statistics and mean  $\pm$  SEM values, respectively.

To test for causality, we performed a pathway-specific chemogenetic inhibition of the PiC-to-mPFC pathway during the conspecific interaction and recorded NAc projectors 24 hours later. Observer mice were first injected in the mPFC with the retrograde AAV2rg-pgk-Cre virus, followed by an injection in the PiC of an AAV that expresses, in a cre-dependent manner, the hM4D(Gi) receptor (16). During the same surgery, the AAV-ChR2-EYFP was injected in the PiC and 30 days later, CTB-555 was injected in the NAc to label mPFC NAc projectors (Fig. 4, A and B). Application of CNO decreased neuronal excitability and evoked an outward current that was reversed by the potassium channel blocker barium (fig. s4, G to I). Whereas CNO (2 mg/kg, intraperitoneally [ip]) injected in an observer mouse before conspecific interaction did not affect the time spent with the demonstrators (Fig. 4C), ex vivo recordings of light-evoked currents in mPFC NAc projectors revealed that uncued and cued observer mice had similar EPSC/IPSC and AMPA/NMDA ratios (Fig. 4, D and E). Finally, we tested whether chemogenetic inhibition of the PiC-to-mPFC pathway during conspecific interaction could affect STFP expression (Fig. 4F). Injection of CNO in the absence of hM4D(Gi) receptors did not alter the change in preference for cumin-scented food during the food choice session. Conversely,

silencing the activity of PiC-to-mPFC pathway in cued observers during conspecific interaction abolished STFP expression (Fig. 4G), without affecting the total amount of food eaten (fig. s5A). Cued mice with the PiC-to-mPFC pathway inhibited during a food choice session showed a similar preference score compared with uncued animals (fig. s5B). If STFP-induced potentiation at PiC-to-mPFC NAc projectors is essential for STFP expression, then depotentiating these synapses in vivo after STFP acquisition should also revert the cumin preference in cued observers. To test this prediction, we induced a long-term depression in vivo of the PiC-to-mPFC pathway by photostimulating ChR2-expressing PiC terminals in the mPFC at 1 Hz, 24 hours after STFP acquisition, a protocol able to robustly reverse potentiated excitatory synapses (11, 17) and validated in mPFC slices (fig. s5C). When tested 4 hours later in a food choice session, a preference index similar to that of control animals was observed (Fig. 4, H and I).

Here, we delineate the circuit that underlies the transmission of a food safety signal emanating from a conspecific that affects the choice of the consumption of an unfamiliar flavor. After the detection of the specific odor and the semiochemical CS<sub>2</sub> in the olfactory bulb (2), the message activates a set of PiC neurons. Consistent

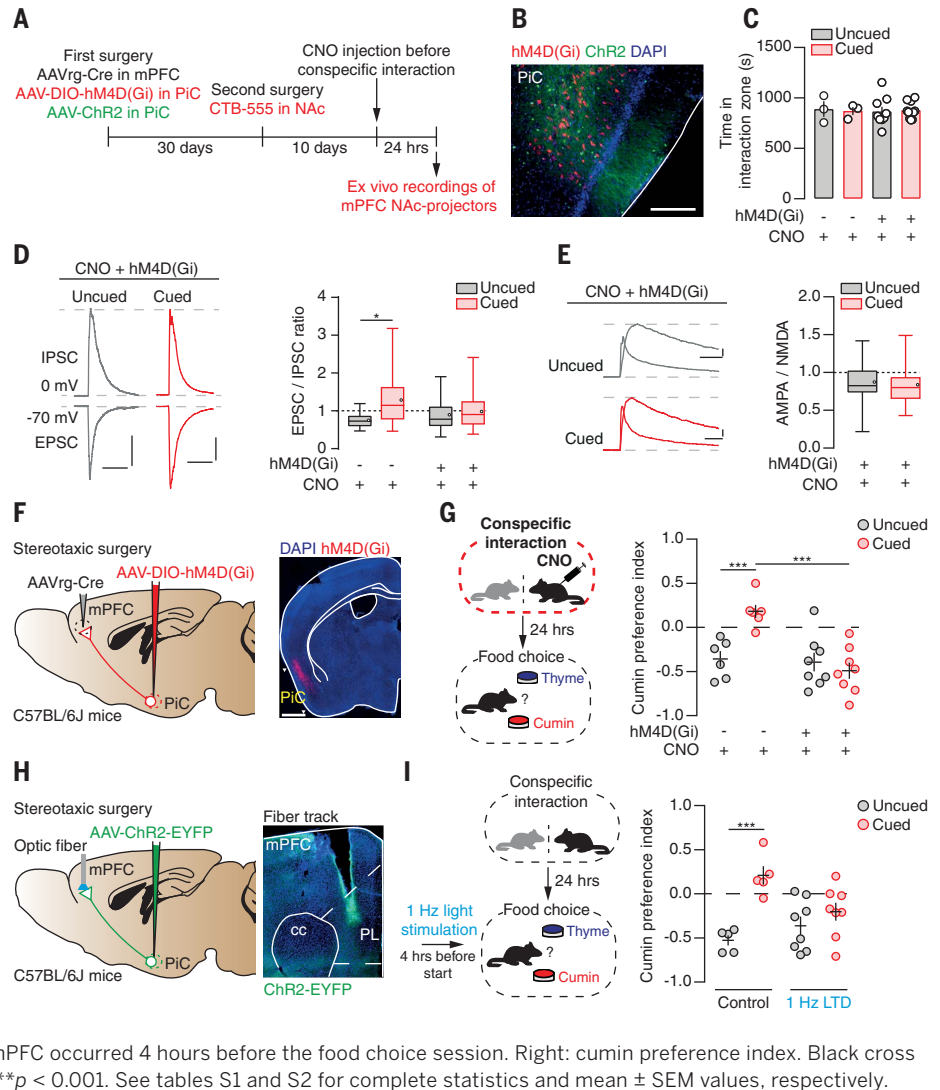
with a study that identified ensembles coding for specific odors (18, 19), similar mechanisms may be functioning here to ensure specificity. Activity in the PiC then drives a potentiation of excitatory afferents onto neurons in the mPFC that project to the NAc. As a result, the MSNs may increase the baseline firing frequency, which, when inhibited during decision making, allows for a higher dynamic range of the response. Alternatively, the enhanced excitation and increased activity in the pathway serves to suppress consumption of the preferred option, rather than (or in addition to) promoting selection of a new, nonpreferred choice.

Monitoring the activity of these neurons in vivo will determine the induction mechanism in the mPFC and the synaptic partners of the NAc projectors, which then drive the behavior through temporally precise activity patterns. Microinfusion of pharmacological agents clearly implicates glutamate transmission in a moment-by-moment control of intake (20). More generally, the mPFC neurons may also integrate additional conspecific signals in modalities other than olfaction to convey more complex social information and steer choices, such as aggression or mating.

Our results identify the PiC-to-mPFC neurons targeting the NAc as being essential for food preference driven by an olfactory cue in a social

#### Fig. 4. Inhibition of the PiC-to-mPFC pathway during conspecific interaction prevents STFP expression.

**(A)** Virus injection strategy for PiC-to-mPFC chemogenetic inhibition and optogenetic stimulation of PiC terminals in the mPFC. **(B)** Example of PiC-to-mPFC neurons infected with hM4D(Gi) and Chr2. Scale bar, 200  $\mu\text{m}$ . **(C)** Inhibition of the PiC-to-mPFC pathway did not reduce the time spent by uncued and cued mice with the demonstrators. **(D)** Example of EPSC and IPSC after inhibition of PiC-to-mPFC pathway during conspecific interaction (left). Scale bars: 100 pA, 100 ms. When the PiC-to-mPFC pathway was inhibited, EPSC/IPSC ratios were similar between uncued (30 cells from five mice) and cued (30 cells from five mice) groups (right). For the control groups: 15 cells (three mice) and 16 cells (three mice) were recorded from uncued and cued animals, respectively. **(E)** Example trace of AMPA-EPSCs recorded at +40 mV after PiC-to-mPFC inhibition and grouped data for AMPA/NMDA ratio (right). Scale bars: 100 pA, 50 ms. 16 and 19 cells were recorded from four uncued and five cued mice, respectively. **(F)** Viral strategy with histological examples for chemogenetic inhibition of PiC-to-mPFC. Scale bar, 500  $\mu\text{m}$ . **(G)** Left: CNO injection (2 mg/kg, ip) was performed 60 min before the conspecific interaction in uncued and cued observers. Right: impact of PiC-to-mPFC pathway inhibition during the conspecific interaction on the cumulin preference score. **(H)** Surgery strategy with histological example showing the track of the optic fiber targeting the mPFC. **(I)** Left: in vivo photostimulation of PiC terminals in the mPFC occurred 4 hours before the food choice session. Right: cumulin preference index. Black cross represents mean  $\pm$  SEM. \* $p < 0.05$ ; \*\* $p < 0.01$ ; \*\*\* $p < 0.001$ . See tables S1 and S2 for complete statistics and mean  $\pm$  SEM values, respectively.



context. By combining viral injection strategies and electrophysiological recordings, we demonstrate that STFP acquisition increases the excitatory transmission at PiC-to-NAc projectors in the mPFC, which is the cause of the altered behavior. Our study thus adds a circuit to the complexity of food intake behavior that may override immediate metabolic needs in the interest of survival.

#### REFERENCES AND NOTES

- H. Zheng, N. R. Lenard, A. C. Shin, H. R. Berthoud, *Int. J. Obes.* **33** (Suppl 2), S8–S13 (2009).
- S. D. Munger *et al.*, *Curr. Biol.* **20**, 1438–1444 (2010).
- J.-F. Gariépy *et al.*, *Front. Neurosci.* **8**, 58 (2014).
- B. Bessières, O. Nicole, B. Bontempi, *Nat. Protoc.* **12**, 1415–1436 (2017).
- Z. Liu *et al.*, *Neuron* **95**, 106–122.e5 (2017).
- J. M. Otis *et al.*, *Nature* **543**, 103–107 (2017).
- D. R. Euston, A. J. Gruber, B. L. McNaughton, *Neuron* **76**, 1057–1070 (2012).
- E. C. O'Connor *et al.*, *Neuron* **88**, 553–564 (2015).
- E. Lesburguères *et al.*, *Science* **331**, 924–928 (2011).
- A. Friedman *et al.*, *Cell* **161**, 1320–1333 (2015).
- Y. Zhu, C. F. R. Wienecke, G. Nachtrab, X. Chen, *Nature* **530**, 219–222 (2016).
- C. J. Guenther, K. Miyamichi, H. H. Yang, H. C. Heller, L. Luo, *Neuron* **78**, 773–784 (2013).
- L. Ye *et al.*, *Cell* **165**, 1776–1788 (2016).
- L. A. Schwarz *et al.*, *Nature* **524**, 88–92 (2015).
- S. Cull-Candy, L. Kelly, M. Farrant, *Curr. Opin. Neurobiol.* **16**, 288–297 (2006).
- T. J. Stachniak, A. Ghosh, S. M. Sternson, *Neuron* **82**, 797–808 (2014).
- V. Pascoli, M. Turiault, C. Lüscher, *Nature* **481**, 71–75 (2011).
- D. D. Stettler, R. Axel, *Neuron* **63**, 854–864 (2009).
- B. Roland, T. Deneux, K. M. Franks, B. Bathellier, A. Fleischmann, *eLife* **6**, e26337 (2017).
- C. S. Maldonado-Irizarry, C. J. Swanson, A. E. Kelley, *J. Neurosci.* **15**, 6779–6788 (1995).

#### ACKNOWLEDGMENTS

We thank E. C. O'Connor and all the lab members for comments on the manuscript. We also thank Alan Carleton and Ivan Rodriguez for critical comments on the manuscript. **Funding:** This work was supported by the Swiss National

Science Foundation (core grant 310030B\_170266 to C.L. and Ambizione grant P200P3-154737 to P.V.) and by an advanced grant from the European Research Council (MeSSI) (to C.L.). **Author contributions:** M.L. conceived the experiments and performed surgeries for viral infection, behavioral experiments, and electrophysiological recordings. R.A. and T.S. performed immunohistological staining and histological analysis. J.F. and R.V.Z. performed data analysis. V.P. performed patch recordings. C.L. conceived and supervised the study and wrote the manuscript with M.L. **Competing interests:** C.L. is a member of the scientific advisory boards of Stalicia SA and the Phénix and IRP Foundations. **Data and materials availability:** All data and materials used in the analysis are available in the main text and supplementary materials.

#### SUPPLEMENTARY MATERIALS

science.sciencemag.org/content/364/6444/991/suppl/DC1  
Materials and Methods  
Figs. S1 to S5  
Tables S1 and S2  
Reference (21)

7 January 2019; accepted 16 May 2019  
10.1126/science.aaw5842

## Social transmission of food safety depends on synaptic plasticity in the prefrontal cortex

Michaël Loureiro, Ridouane Achargui, Jérôme Flakowski, Ruud Van Zessen, Thomas Stefanelli, Vincent Pascoli and Christian Lüscher

*Science* **364** (6444), 991-995.  
DOI: 10.1126/science.aaw5842

### This is safe, you can eat it

Social transmission of food preference is a model for studying nonspatial memory. In mice, a signal that food is safe to eat is transmitted by its smell along with molecules in the breath of a conspecific. How the odor itself is encoded and assigned valence is poorly understood. Loureiro *et al.* found a monosynaptic pathway between two brain areas, the piriform cortex and the medial prefrontal cortex, that plays a central role in this process. This connection strengthens during social interaction, thereby allowing a mouse to provide a food safety message to its companion.

*Science*, this issue p. 991

#### ARTICLE TOOLS

<http://science.sciencemag.org/content/364/6444/991>

#### SUPPLEMENTARY MATERIALS

<http://science.sciencemag.org/content/suppl/2019/06/05/364.6444.991.DC1>

#### REFERENCES

This article cites 21 articles, 2 of which you can access for free  
<http://science.sciencemag.org/content/364/6444/991#BIBL>

#### PERMISSIONS

<http://www.sciencemag.org/help/reprints-and-permissions>

Use of this article is subject to the [Terms of Service](#)

---

*Science* (print ISSN 0036-8075; online ISSN 1095-9203) is published by the American Association for the Advancement of Science, 1200 New York Avenue NW, Washington, DC 20005. The title *Science* is a registered trademark of AAAS.

Copyright © 2019 The Authors, some rights reserved; exclusive licensee American Association for the Advancement of Science. No claim to original U.S. Government Works